A R T I C L E

An amino-based protic ionic liquid as a corrosion inhibitor of mild steel in aqueous chloride solutions

Tobias Eduardo Schmitzhaus[1,2] | **Maria R. Ortega Vega**[1] | **Roberto Schroeder**[1,3] | **Iduvirges Lourdes Muller**[1] | **Silvana Mattedi**[4] | **Célia de Fraga Malfatti**[1]

[1]Department of Metallurgy, Laboratório de Pesquisa em Corrosão (LAPEC), Universidade Federal do Rio Grande do Sul (UFRGS), Porto Alegre, Rio Grande do Sul, Brazil

[2]Department of Metallurgy, Instituto Federal de Mato Grosso do Sul, Corumbá, Brazil

[3]Department of Mechanical Engineering, Pontifícia Universidade Católica do Rio Grande do Sul (PUCRS), Porto Alegre, Rio Grande do Sul, Brazil

[4]Department of Chemical Engineering, Laboratório de Termodinâmica Aplicada, Universidade Federal da Bahia (UFBA), Salvador, Bahia, Brazil

Correspondence
Tobias Eduardo Schmitzhaus,
Department of Metallurgy, Laboratório de Pesquisa em Corrosão (LAPEC), Universidade Federal do Rio Grande do Sul (UFRGS), Avenida Bento Goncalves 9500, Porto Alegre – RS 91501-970, Brazil.
Email: tobiasschmitzhaus@gmail.com and tobias.schmitzhaus@ifms.edu.br

Funding information
Coordenação de Aperfeiçoamento de Pessoal de Nível Superior, Grant/Award Number: 88887.463867/2019-00; Conselho Nacional de Desenvolvimento Científico e Tecnológico, Grant/Award Numbers: 155274/2018-0, 306640/2016-3, 307723/2018-6

Abstract
Protic ionic liquids (PILs) have shown to be promising substances as corrosion inhibitors (CIs). In line with this, the aim of this study is to study the performance and propose the corrosion inhibition mechanism of N-methyl-2-hydroxyethylamine (M-2HEAOL) and bis-2-hidroxyethylamine (B-HEAOL) oleate, for mild steel, in a neutral chloride solution. Electrochemical characterization was conducted under static and hydrodynamic conditions, and it was revealed that M-2HEAOL and B-HEAOL worked as mixed-type CIs with more interference on the anodic reaction. Inhibition efficiency depended on the concentration reaching 97% of inhibition efficiency in 5 mmol/L concentration. Scanning electron microscopy, optical interferometry, Raman spectroscopy, and Fourier-transform infrared spectroscopy are used to elicit the chemical composition of the surface film and corrosion morphology of steel in the presence of CIs, the adsorption processes of which involved physical and chemical adsorption between metal and different parts of ionic liquids. The results allowed the proposition of a corrosion inhibition mechanism.

K E Y W O R D S
carbon steel, corrosion inhibition, electrochemical techniques, protic ionic liquid, surface analysis

1 | INTRODUCTION

Steel has a wide range of applications due to the versatility of its mechanical properties and its low cost. In many of its uses, such as heat exchangers, cooling water systems and industrial boilers, it is in contact with aqueous solutions where it is prone to corrosion.[1–3] To increase the life of these devices to the maximum possible, preventing them from critical failures due to corrosion especially in chloride-containing media, many techniques can be applied, and among them, corrosion inhibitors (CIs) are very popular. A CI is a substance that

when added to an electrolyte is able to minimize anodic and/or cathodic reactions, preventing or mitigating the corrosion process.[4–6]

Unfortunately, some of these inhibitors are toxic to living beings or to the environment,[7,8] especially chromate-based ones.[9] The toxicity can be manifested in their application or in the synthesis phase,[10] and also during disposal, pointing to the need for safer alternatives. As a consequence, the industrial sector is following the trend to not only look for efficient and stable CIs but also to pay attention to environmental aspects.[11–13] Organic compounds exhibiting functional groups with nitrogen, sulfur, oxygen and phosphorus heteroatoms, and/or π-electron,[11,14–16] may facilitate their chemisorption and/or physisorption on metallic surfaces creating a protective barrier; thus, such compounds have been investigated as potential inhibitors for various metals in different environments, mainly in acidic solutions.

As for the scientific and industrial branches, the use of protic ionic liquids (PILs) as CIs has become very interesting due to their unique possibility of properties such as low volatility, wide liquidus range, high thermal and chemical stability, ionic conductivity, low toxicity, and no combustibility.[11,17,18] These compounds consist of organic salts (organic cations and organic/inorganic anions) with at least one motile proton, in charge to promote the formation of hydrogen bonds[18–20] and are in the liquid phase at room temperature or close to it.[21] PILs can be adapted to a specific application, from their structural design, developing specific properties by modifying the cation and/or anion structure.[22,23]

Corrosion-inhibiting properties of compounds that contain functional groups such as amine and carboxylic acid were reported, as Zhang et al.,[24] Yoo et al.,[12] Amin et al.,[25] and Amin and Ibrahim[26] have shown in their research using mild steel and cold rolled steel in different acid media, showing promising results related to anticorrosion effects. Chong et al.[1] tested some protic imidazolium cation and a 4-hydroxycinnamate anion as a CI for mild steel in 0.01 mol/L sodium chloride media and reached a maximum of 86% inhibition efficiency. Arellanes-Lozada et al.[11] used ammonium-based ionic liquids (methyltrioctylammonium methyl sulfate and others) to inhibit corrosion of API-X52 steel in 1 mol/L hydrochloric acid solution, showing that ionic liquids worked as mixed-type CIs. Mashuga et al.[21] studied some ionic liquids (1-hexyl-3-methylimidazolium trifluoromethanesulfonate and others) as CIs for mild steel in 1 mol/L hydrochloric acid solution and suggested the formation of Fe/ILs complexes in the inhibiting mechanism.

As no works have been found on corrosion inhibition by amino PILs in neutral media, the objective of this study was to evaluate the inhibition effect on AISI 1020 steel in neutral 0.01 mol/L sodium chloride aqueous solutions of two PILs derived from two secondary amines (*N*-methyl-2-hydroxyethylamine [M-2HEAOL] and bis-2-hidroxyethylamine [B-HEAOL]) and oleic acid. Different hydrodynamic conditions were used for electrochemical characterization, with the aim to evaluate the influence of hydrodynamic flow on the corrosion behavior of mild steel. The set of results obtained was used to propose a corrosion inhibition mechanism involving PILs in neutral chloride medium.

2 | EXPERIMENTAL SECTION

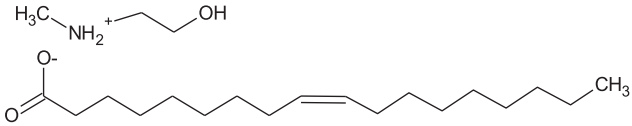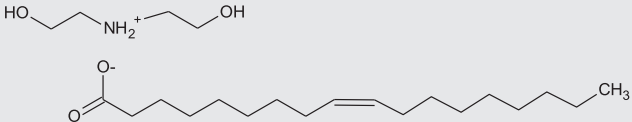### 2.1 | Materials and samples preparation

The chemical composition of mild steel used in the experiments (wt%) was C (0.03%), Si (0.008%), Mn (0.23%), P (0.014%), S (0.005%), Cr (0.007%), Al (0.03%), B (0.0006%), and Fe for balance. Disc specimens, 27 mm (diameter) × 1.4 mm (thickness), were used for surface analysis and electrochemical measurements with static electrodes; for linear polarization resistance (LPR) measurements, a rotating cylinder electrode (LPR/RCE) of 11 mm diameter and 35 mm length was used. The exposed surface area of flat specimens was 2.83 cm^2, while the remainder was wrapped with galvanic tape 3MTM; for LPR/RCE, 3.47 cm^2 surface-exposed area was used. Before all measurements, the specimens were mechanically abraded with emery paper up to 1,200 grit, then rinsed with distilled water, degreased in a neutral soap solution, acetone, alcohol and deionized water, and dried with fresh air.

All experiments were carried out in naturally aerated, 0.01 mol/L sodium chloride p.a. the solution used blank or prepared in the presence of various concentrations of PILs ranging from 5×10^{-4} to 5×10^{-3} mol/L proposed as CIs, as shown in Table 1. This chloride concentration was chosen because it is common in heat exchangers, cooling water systems, and industrial boilers.[1–3] These are the subject of patent BR 10 2019 015605-8 and were reported as lubricants for aluminum by Ortega Vega et al.[23]

2.2 | Dissolved oxygen, pH, and conductivity

Dissolved oxygen of the solutions was determined with an AKSO ECO-04-1017 meter; conductivity was measured with a Bel Engineering model W12D conductivity meter and pH was measured with a Sanxin MP521 Lab pH/conductivity meter at room temperature (25°C).

TABLE 1 Structures of the studied protic ionic liquids (PILs)[23]

PIL	Structure
M-2HEAOl (*N*-methyl-2-hydroxyethylammonium) oleate	
B-HEAOl (bis-2-hydroxyethylammonium) oleate	

2.3 | Electrochemical measurements

A conventional three-electrode cell assembly with a mild steel working electrode, a saturated calomel reference electrode (SCE), and a platinum wire counter electrode were used for electrochemical measurements, using the Autolab 302N potenciostat/galvanostat. All tests were conducted at least in triplicate to guarantee reproducibility. Before the experiments, the working electrode was immersed in the test solution for 30 min to reach steady-state and open-circuit potential (E_{OCP}) was monitored. Tests were conducted open to the atmosphere at room temperature ($25 \pm 1°C$). To avoid the influence of oxide layers, potentiodynamic polarization curves were performed first from E_{OCP} in cathodic direction until -250 mV versus E_{OCP}; then samples were left to reach OCP and, after stabilization, the potential was scanned from E_{OCP} in an anodic direction until $+450$ mV versus E_{OCP} with a scan rate of 1.0 mV/s. Data were collected by electrochemical software NOVA ver2.1.4.[27,28]

The inhibition efficiency ($\eta\%$) was calculated using the following:

$$\eta(\%) = \frac{i_{corr}^0 - i_{corr}^i}{i_{corr}^0} \times 100, \tag{1}$$

where i_{corr}^0 and i_{corr}^i are the values of corrosion current density in the absence and presence of inhibitor, respectively.

The influence of hydrodynamic flow on the corrosion behavior of mild steel in the inhibited (5×10^{-3} mol/L of PIL) and uninhibited solutions was investigated using the rotating electrode module PINE model AFASR. The samples were tested by LPR technique obtained in the potential range -15 to $+15$ mV (vs. E_{OCP}) with a scan rate of 0.1 mV/s, to carry out the measurement under steady-state conditions.[28] Tests were performed using RCE at rotation speeds of 250, 500, 1,000, and 2,000 rpm for 1 hr long each, following ASTM G59-97, 2014[29] and ASTM G185-06, 2016.[30]

Cyclic voltammetry was performed to demonstrate the presence of adsorbed species on the working electrode to elucidate the corrosion-inhibiting mechanism. The scanning rate is very important in this type of determination. Faster sweeping rates lead to a decrease in the size of the diffusion layer; consequently, higher currents are observed.[31,32] For the electrochemically reversible electron transfer processes involving free-diffusion redox species, the Randles–Sevcik equation (2) describes the linear peak current i_p, increase (in amperes) with the square root of the sweep rate v (V/s), where n is the number of electrons transferred in the redox event, A (cm^2) is the surface area of the electrode (usually treated as the geometric surface area), D_o (cm^2/s) is the diffusion coefficient of the oxidized or reduced analyte, and C_0 (mol/cm^3) is the concentration of the analyte.[33]

$$i_p = 0.446n\, FAC_0 \left(\frac{nFvD_0}{RT} \right). \tag{2}$$

The Randles–Sevcik equation can provide indications as to whether an analyte is diffusing freely in solution or not.

For reversible electron transfer processes involving free redox species to diffuse, the Randles–Sevcik equation describes the dependence of the current peak by the scan rate as the plot of i_p versus $v^{1/2}$ being linear. On the other hand, for species adsorbed on the electrode, the current response is described as

$$i_p = \frac{n^2 F^2}{4RT} vA\Gamma, \tag{3}$$

where Γ is the coverage of the species adsorbed in mol/cm^2. The current response of an adsorbed species should vary linearly with v. For testing that, scans of -0.9 to $+0.9$ V versus SCE using platinum as the working electrode, platinum as the counter electrode and a SCE, with scan rates of 150, 120, 100, 80, 50, 30, 20, 10 mV/s were performed. The peak currents were plotted against v and $\sqrt{v}$ to obtain information of adsorption.[31]

2.4 | Surface analysis

Surface analysis of the samples was done after corrosion tests, in an scanning electron microscopy JEOL JECM 6060 microscope and by Bruker ContourGT-K optical interferometer (green light) to give quantitative information of corrosion morphology.

A homemade contact angle tester with 0.7 μl liquid drop evaluated contact angles of 0.01 mol/L sodium chloride solution with and without inhibitors on steel. A digital camera recorded the shapes of droplets and the angles were calculated using Surftens 4.5 software. The contact angle data were obtained from the average of five records in the same condition.

A Renishaw inVia Spectrometer System for Raman spectral analysis (and Fourier-transform infrared spectrometer [FTIR] in attenuated total reflection [ATR] Nicolet IS10 Thermo Scientific was used to study chemical components on metal surface after 20 days of immersion in 0.01 mol/L sodium chloride +5 mmol/L M-2HEAOl.

3 | RESULTS AND DISCUSSION

3.1 | Solution characteristics

Table 2 shows the conductivity of solutions that did not undergo significant changes in the range of concentrations tested. As for dissolved O_2, there were no marked changes either, showing that ionic liquids have no influence on the amount of dissolved oxygen in the tested concentration range. This does not necessarily indicate that the electrochemical reactions involving O_2 occur at the same rate, once among other factors, the diffusion coefficient directly affects the oxygen reduction limiting current, so if PILs affect this property there may be changes in the O_2 limiting current.[4]

A gradual increase of pH was observed as the amount of ionic liquid in solution was increased as shown in Table 2. For the highest concentration tested (5 mM), a noticeable increase was observed, from 5.73 (0.01 mol/L sodium chloride) to 9.58 and 8.97, for M-2HEAOL and B-HEAOL, respectively. This fact is due to the molecular structure of the liquids having ammonium groups. For application as a CI for steel, this effect may be beneficial, since, according to the Pourbaix diagram, iron can enter a region of passivity at higher pH.[4,34] To clarify the influence of pH in inhibition behavior, electrochemical tests using 0.01 mol/L sodium chloride solution in pH 9 were performed.

When a drop of water is dispensed on the steel surface, molecules already adsorbed on the surface (due a previous 30 min immersion in the studied solutions) can influence the adsorption of water molecules, depending on the hydrophilic/hydrophobic nature of the adsorbed layer present.[35]

Figure 1 shows the water contact angle for clean steel and steel after immersion in the inhibited and uninhibited solution. Clean steel showed a water contact angle of $29 \pm 1°$, which demonstrates that the surface was clean and water was capable of wetting the surface. Similar low values of contact angles ($27 \pm 1°$) were found for steel after immersion in uninhibited solution, which can be due to the presence of hydrophilic corrosion products that caused the water droplets spreading on the metal surface.[35–37]

Besides, Figure 1 shows the water contact angle of the steel plates previously immersed in test solution with B-HEAOL (0.5, 2.5, 5.0 mmol/L and after 20 days of immersion, respectively) and M-2HEAOL (0.5, 2.5, 5.0 mmol/L and after 20 days of immersion, respectively). For all concentrations, an important increase in the water contact angle was observed compared with the uninhibited electrolyte. The obtained angles were equal or higher than 90°, which shows the hydrophobic characteristics of the steel surface. At higher contact angles, it becomes harder for the liquid to wet the surface, which consequently hinders the interaction of corrosive agents and the metallic substrate.[38]

The observed surface hydrophobicity can be ascribed to ionic liquid molecules adsorbing on the steel, which may be related to the amphiphilic character of the studied PILs, which are structures that have one hydrophilic part and another part hydrophobic. According to Álvarez et al.,[39,40] in these ionic liquids, alkyl chains of anion molecules behave hydrophobic, while the polar carboxylate anion head behaves hydrophilic, as well as the cation moiety. In addition, it is possible to attribute a relationship between the PIL concentration in solution and the contact angle; in other words, the contact angle increased with the increase of PIL concentration in the electrolyte. This implies that hydrophobicity of the steel surface is influenced by the concentration of the inhibitor, where an increase in the inhibitor concentration increases the hydrophobic nature of the substrate.[41] From the contact angle observations, it is evident that the presence of PILs has changed the surface wettability of steel by adsorbing at the steel surface.

In addition, after 20 days of immersion, the contact angle increased compared with the same situation in 30 min of immersion, which indicates that PILs are actuating over time and giving a more hydrophobic characteristic to the steel surface.

3.2 | OCP measurements

The variation of OCP with immersion time for steel in 0.01 mol/L sodium chloride in the presence and absence

TABLE 2 pH, conductivity, and dissolved oxygen data for the tested solutions (standard deviation in parenthesis)

	pH	Conductivity (µS)	Dissolved oxygen (mg/L)
0.01 mol/L NaCl	5.73 (0.04)	838 (9.71)	6.45 (0.43)
M-2HEAOL 0.25 mM	8.36 (0.05)	844 (7.23)	5.66 (0.33)
M-2HEAOL 0.50 mM	8.60 (0.07)	842 (4.36)	5.64 (0.08)
M-2HEAOL 1.5 mM	9.33 (0.09)	855 (3.33)	5.70 (0.21)
M-2HEAOL 2.5 mM	9.42 (0.03)	860 (1.73)	5.74 (0.34)
M-2HEAOL 5.0 mM	9.58 (0.02)	854 (8.02)	5.74 (0.34)
B-HEAOL 0.25 mM	7.91 (0.06)	855 (4.61)	6.63 (0.77)
B-HEAOL 0.50 mM	8.26 (0.04)	845 (1.53)	6.61 (0.81)
B-HEAOL 1.5 mM	8.56 (0.02)	849 (3.52)	6.38 (0.60)
B-HEAOL 2.5 mM	8.51 (0.01)	866 (7.00)	6.30 (0.66)
B-HEAOL 5.0 mM	8.97 (0.01)	840 (3.06)	6.37 (0.77)

Abbreviations: B-HEAOL, bis-2-hidroxyethylamine; M-2HEAOL, N-methyl-2-hydroxyethylamine.

of PILs in all the studied concentrations at 25°C is shown in Figure 2a,b. When clean steel is exposed to dry air, it is usually covered with a transparent oxide film, but then if the steel is placed in an aggressive environment such as chloride solutions, corrosion accompanied by a loss of the air-formed film takes place, which can be recognized by a drop in potential.[42] Such behavior was found for steel in uninhibited solution (0.01 mol/L sodium chloride, pH 6). In the first seconds, it is possible to identify this thin air-formed oxide layer by a relatively high OCP. After a few seconds, the OCP dropped down constantly, since there is a loss of air-formed oxide layer, with onset iron dissolution and formation of corrosion product.[42] Chloride ions have a particular influence on this breakdown, it being well accepted that the amount of chloride ions is directly related to how fast this breakdown occurs. This is probably caused by the attraction of Cl^- ions toward steel speeding up the breakdown and formation of corrosion products, as stated by Gabrielli et al.[42,43] and Liengen et al.[44]

The results for 0.01 mol/L sodium chloride, pH 9 are also shown in Figure 2a,b. The behavior is similar to that of uninhibited steel in the presence of chloride solution in pH 6, with only one particular difference, the time to breakdown the air-formed oxide was longer at pH 9. In other words, the increase in pH influenced the stability of the air-formed oxide layer.

The steel immersed in the sodium chloride solution containing PILs, from 1.5 to 5 mmol/L for both PILs (M-2HEAOL and B-HEAOL), showed more stable OCP values. This phenomenon can be attributed to the adsorption of PILs on the metal surface.[36] The OCP shifted in the positive direction compared with that of the uninhibited steel, which may have several causes: In this case, it is probably caused by anodic reaction inhibition, due the adsorption of PILs on steel surface,[45] which will be confirmed by polarization and further tests. As for both PILs concentrations of 0.25 and 0.5 mmol/L, the covering probably was not enough to protect the surface steel and the Cl^- ions were capable of reaching the surface and promoting corrosion in some critical points dropping down de OCP values. As most parts of the systems was stable along 1,800 s, this immersion time was used for further electrochemical essays.[46]

3.3 | Potentiodynamic polarization measurements

Potentiodynamic polarization curves were carried out to gain knowledge about the kinetics of cathodic and anodic reactions.[47] The polarization curves for steel in 0.01 mol/L sodium chloride with and without different concentrations of M-2HEAOL and B-HEAOL at 25°C are shown in Figure 2c,d. In the case of cathodic curves, for
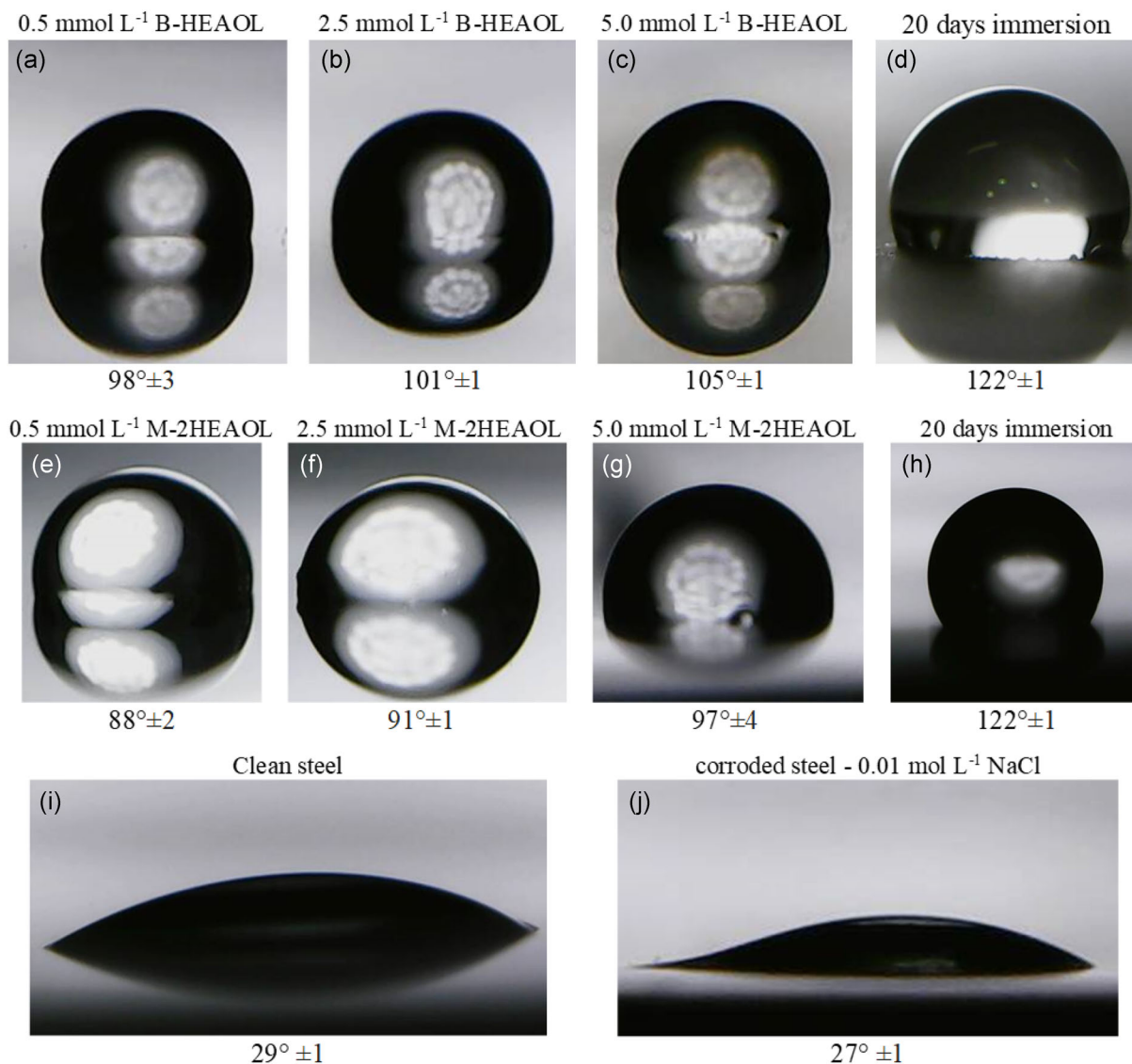
FIGURE 1 Contact angle images for steel before and after contact with 0.01 mol/L sodium chloride + protic ionic liquids [Color figure can be viewed at wileyonlinelibrary.com]

both B-HEAOL and M-2HEAOL, a small shift is observed in current densities and a little change in curves shapes. The lower current densities for both studied PILs (B-HEAOL and M-2HEAOL) may be attributed to the adsorbed PILs blocking part of the active metal surface.

Corrosion potential changes toward positive values (anodic direction) were observed and are mainly due to the anodic reaction's polarization in all studied cases; these alterations were in a range of change of 30–190 mV depending on PIL concentration. The classification of a compound as an anodic or cathodic inhibitor is feasible when the OCP shift is at least 85 mV with respect to the one measured in the blank solution.[48–50] Moreover, the polarization curves show that both anodic and cathodic reactions are affected but the effect on the anodic reactions is

much more prominent. Thus, the studied inhibitor acted as a mixed type, but predominantly as an anodic inhibitor.[47]

The corrosion current densities (i_{corr}) were obtained from the polarization curves by Tafel extrapolation of the cathodic branch to the corrosion potential which gives the net rate of the cathodic reaction at the corrosion potential; but from Wagner and Traud theory,[51] this is also the net rate of the anodic reaction at the corrosion potential. This method was used because the anodic branch is not under activation control, a condition that must be obeyed to use the Tafel method.[52] de Assis et al.[53] used similar strategy in their studies. Also, oxygen cathodic reaction has diffusion control issues, but in this studied case, the potential where the limiting current is observed far from corrosion potential, so, close
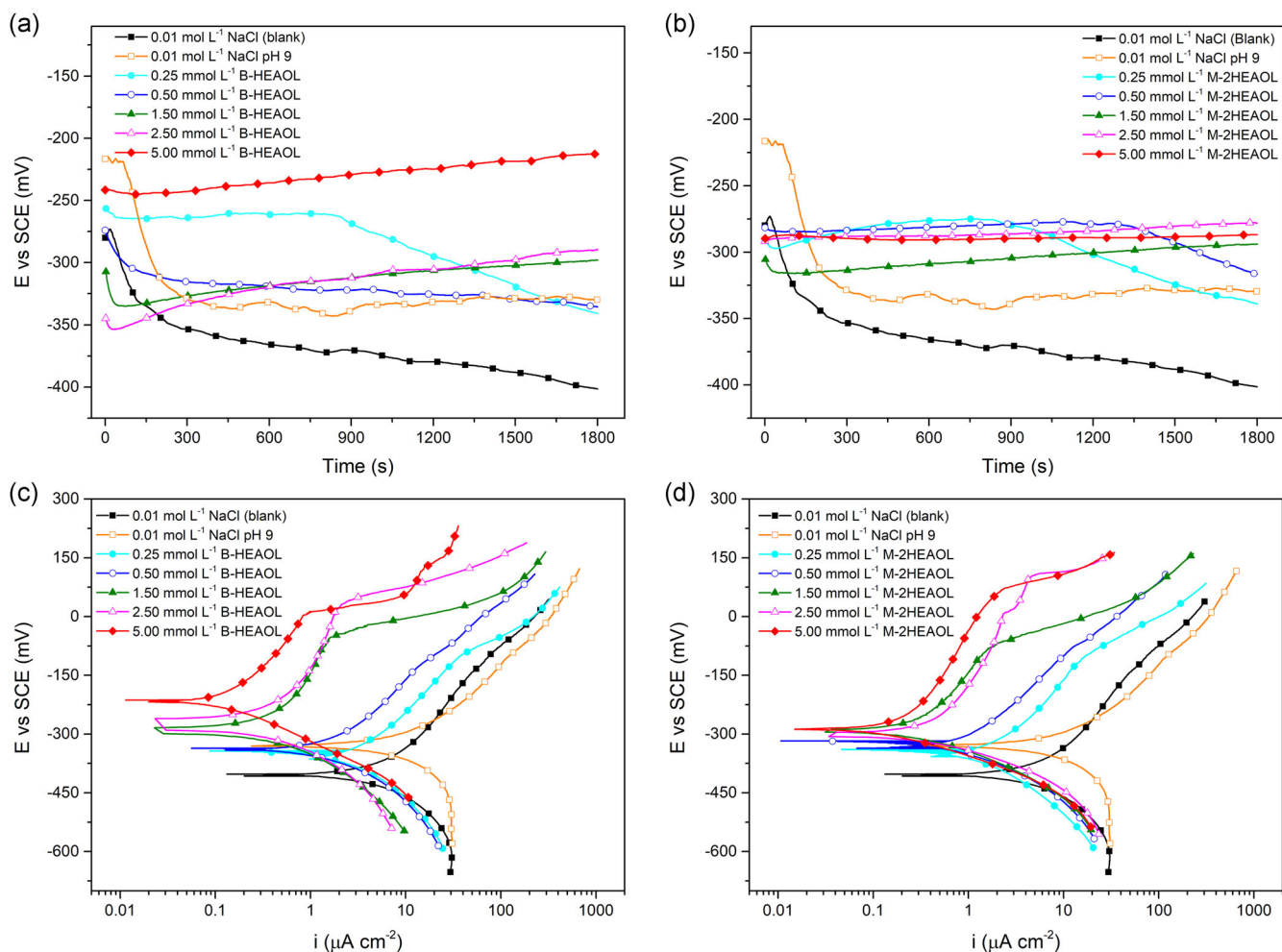
FIGURE 2 Open-circuit potential measurements for steel in 0.01 mol/L sodium chloride in the presence and absence of (a) *N*-methyl-2-hydroxyethylamine (M-2HEAOL) and (b) bis-2-hidroxyethylamine (B-HEAOL); (c) polarization curves of steel in 0.01 mol/L sodium chloride + B-HEAOL solution and (d) polarization curves of 0.01 mol/L sodium chloride + M-2HEAOL solution [Color figure can be viewed at wileyonlinelibrary.com]

to corrosion potential activation control is expected. Zou et al.[28] found similar results in their studies.

Anodic polarization curves (Figure 2c,d) present a passive behavior in the presence of B-HEAOL and M-2HEAOL in 1.5–5.0 mmol/L, which confirms this trend of acting as anodic inhibitor, presenting corrosion current densities of 0.12 μA/cm^2 (Table 3) for both B-HEAOL and M-2HEAOL in 5 mmol/L concentration. The 0.01 mol/L sodium chloride solution presented corrosion a current density value of 3.77 μA/cm^2, which results in 97% inhibition efficiency for M-2HEAOL and B-HEAOL. Other electrochemical parameters are presented in Table 3.

In addition, a passive region is observed with current densities <1 μA/cm^2 over a 300 mV window, which did not occur for uninhibited steel. Also, in Figure 2c,d, a break potential can be identified at approximately −100 mV for 1.5 mmol/L concentration and 0 mV versus SCE

for 2.5 and 5.0 mmol/L concentration for both PILs. This demonstrates the capability of both PILs in suppressing anodic reaction in a way similar to that of a passive layer. For 0.25 and 0.50 mmol/L PIL concentration, uninhibited steel corrosion process starts under OCP conditions and it is not possible to determine it properly.[54]

Part of this action could be due to the elevation of the solution pH, which decreases the potential necessary for an iron oxide formation in aerated solutions.[55,56] To clarify the performance behavior of both inhibitors, polarization curves of steel were obtained in 0.01 mol/L sodium chloride in the absence of PILs in neutral solution (pH 6) and in pH 9 solution, since the addition of PILs increases the solution's pH. So, we investigated if the performance of PILs was just strictly related with pH increase. Figure 2c,d (orange line) shows the profile of those, and it can be seen that the increase of pH did not show any improvement in the corrosion resistance behavior of steel.

3.4 | Adsorption isotherms and thermodynamic calculations

The inhibition efficiency of the organic inhibitors is strictly affected by their adsorption on the surface of the metal. Some factors, such as nature of the aggressive medium, inhibitor structure, species charge distribution and the nature and surface charge of the metal determine the adsorption process; organic inhibitors generally adsorb on the metals by physical or chemical adsorption, which reduces the reaction area susceptible to corrosive attack.[57,58]

To evaluate the adsorption process of ionic liquids on the steel surface, Langmuir, Temkin, and Frumkin adsorption isotherms were tested according to the following equations[59,60]:

$$\text{Langmuir: } \theta/(1 - \theta) = KC, \quad (4)$$

$$\text{Temkin: } \exp(2a\theta) = KC, \quad (5)$$

$$\text{Frumkin: } \log(\theta/(1 - \theta)C) = \log K + a\theta, \quad (6)$$

where θ is the degree of surface coverage obtained from the polarization curves ($\theta = i_{corr}^0 - i_{corr}^i/i_{corr}^0$), C is the molar concentration of inhibitor, K is the adsorption-desorption equilibrium constant, and a the adsorbate interaction parameter.

The three isotherms tested fitted well to the experimental data (Figure 3), indicating that both ionic liquid adsorbed onto the steel surface. For the Langmuir isotherm (Figure 3a), the correlation coefficient (R^2) value obtained was .9998 for both PILs, while for the Temkin (Figure 3b,c) was .9253 and .9275, and Frumkin was .9505 and .9363 for B-HEAOL and M-2HEAOL, respectively. The free energy of adsorption (ΔG_{ads}^0) was calculated from the Langmuir isotherm, since it showed the best correlation with the experimental data, according to the following equation[11]:

$$\Delta G_{ads}^0 = -RT\ln(55.5K_{ads})[kJ/mol], \quad (7)$$

where T is the absolute temperature, R is the universal gas constant and 55.5 represents the water concentration in moles.

The adsorption-desorption equilibrium constant K was determined as 6,622 for B-HEAOL and 9,009 for M-2HEAOL, leading to $\Delta G_{ads}^0 = -31.7$ and -32.5 kJ/mol for M-HEAOl and B-HEAOl, respectively. The negative value of ΔG_{ads}^0 denotes that adsorption is spontaneous.

Also, different studies have suggested that the analysis of ΔG_{ads}^0 helps to establish the type of adsorption between a metal and an inhibitor.[11,61] It is usually accepted that the value of ΔG_{ads}^0 around -20 kJ/mol or higher (lower adsorption energy) indicates electrostatic interaction (physisorption) between the charged metal surface and charged organic molecules in the bulk of the solution. However, ΔG_{ads}^0 values of around -40 kJ/mol or lower (higher adsorption energy) involve charge sharing or charge transfer between the metal surface and organic molecules (chemisorption),[49,62,63] and between -20 and -40 kJ/mol a mixed type of adsorption is expected.[63] Nevertheless, adsorption of the inhibitor molecules on the metallic surface cannot be simply considered as a purely physical or chemical phenomenon.[63] Completely to the possibility of chemisorption, inhibitor molecules are also able to be adsorbed on the metallic surface via physisorption.[64–67]

Since the ΔG_{ads}^0 values were around -30 kJ/mol indicates that adsorption of the PILs have a degree of physisorption along with chemisorption. Therefore, it can be assumed that PILs molecules adsorb on the steel surfaces via a mixed type adsorption phenomenon. It is noteworthy that chemisorption is predominant over physisorption.[63] In other words, steel may develop electrostatic interactions and some charge sharing with PIL molecules.

TABLE 3 Potentiodynamic polarization parameters for mild steel in the absence and presence of the studied PIL's as corrosion inhibitor

Inhibitor	Concentration	i_{corr} (μA/cm^2)	E_{corr} (mV vs. SCE)	η (%)	E break (mV vs. SCE)
	0.01 mol/L NaCl (Blank)	3.77	−408	–	None
	0.01 mol/L NaCl pH 9	3.97	−332	–	None
B-HEAOL	0.25 mmol/L	1.44	−376	62	None
	0.50 mmol/L	1.01	−343	73	None
	1.50 mmol/L	0.26	−285	93	−50
	2.50 mmol/L	0.18	−262	95	25
	5.00 mmol/L	0.12	−218	97	4
M-2HEAOL	0.25 mmol/L	1.11	−365	71	None
	0.50 mmol/L	0.68	−337	82	None
	1.50 mmol/L	0.29	−289	92	−77
	2.50 mmol/L	0.27	−296	93	7
	5.00 mmol/L	0.12	−286	97	60

Abbreviations: B-HEAOL, bis-2-hidroxyethylamine; M-2HEAOL, *N*-methyl-2-hydroxyethylamine; PIL, protic ionic liquid; SCE, saturated calomel electrode.

The Frumkin and Temkin isotherms (Figure 3b,c) also showed a good correlation with experimental data. The positive slope (*a* term) for both isotherms indicates the existence of an attractive lateral interaction in the adsorption layer.[68–70] It is important to mention that this discussion is valid for a specific condition of temperature and time of immersion. Long exposure time may change the way PILs adsorbs.

3.5 | Linear polarization resistance

To better evaluate the studied PILs as inhibitors in a condition closer to industrial application, LPR method coupled to a rotating electrode module was performed to characterize their behavior in hydrodynamic conditions. Tests were performed using 5 mmol/L for both of PILs since it was the concentration with the best results in hydrostatic conditions.

Reynolds number (*Re*) is used to determine whether the flow is laminar or turbulent. It is calculated from the value of rotation speed, which is in the range of 0–2,000 rpm in the present study. The Reynolds numbers were calculated using the following equation[71,72]:

$$Re = \frac{Ud\rho}{\mu} < 200 \text{ for laminar flow}, \quad (8)$$

where U, d, ρ, and μ, are linear velocity (cm/s), the diameter of the RCE in cm, density of the fluid (g/cm^3) and absolute viscosity (g·cm^{-1}·s^{-1}), respectively. The calculated Re values as presented on Table 4 confirm that the experiments were performed under turbulent flow conditions for all speeds tested.

Figure 4 shows the polarization resistance for all rotations with 5 mmol/L of B-HEAOL and M-2HEAOL. Since to get i_{corr} from R_p most of the time is difficult because β_a and β_c can vary during the time, only R_p will be presented since it gives an indirect measure of corrosion rate for the different conditions.[28] It is noticeable the difference between R_p of blank and both
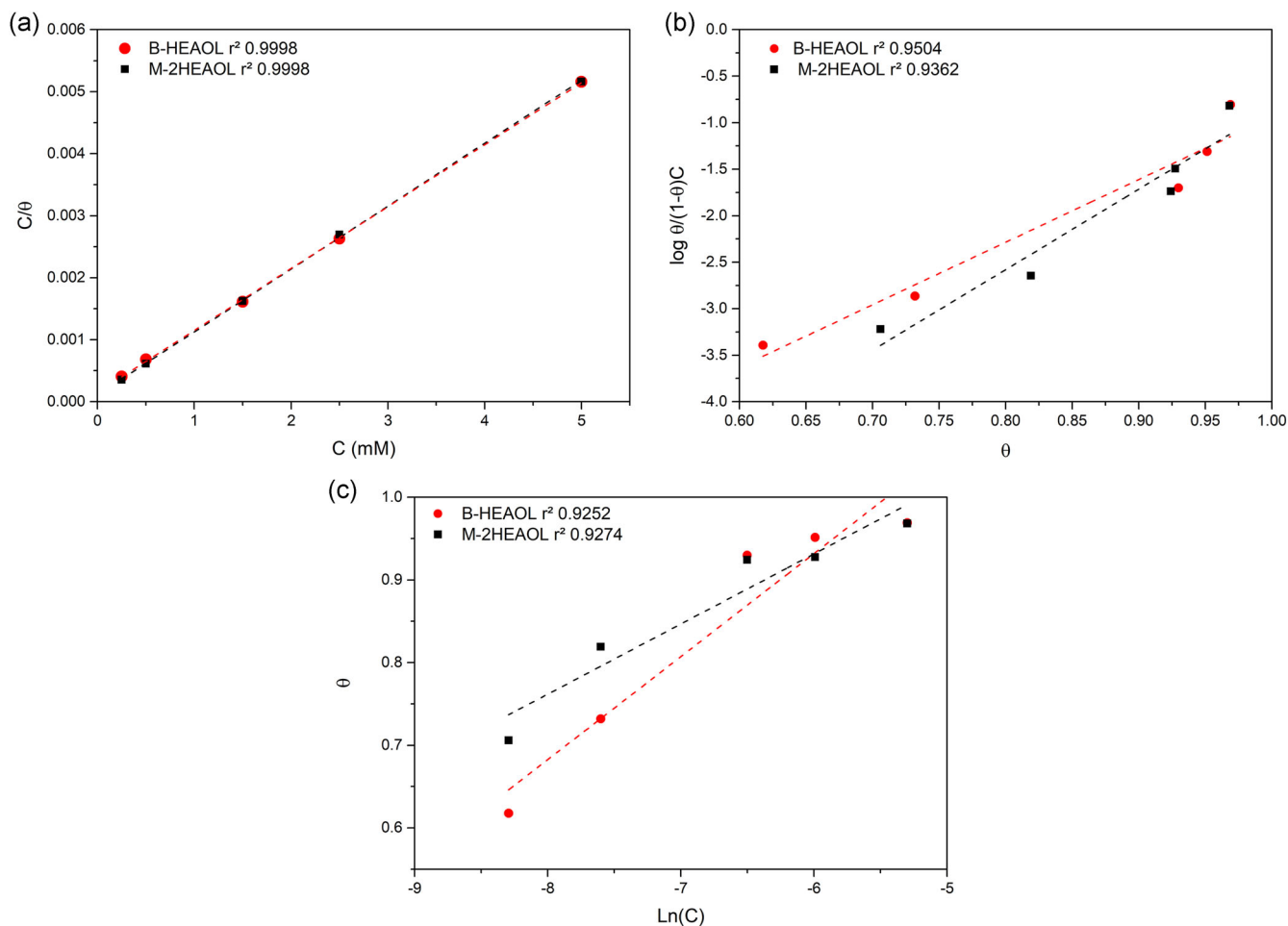
FIGURE 3 (a) Langmuir, (b) Frumkin, (c) Temkin isotherms for the adsorption of bis-2-hidroxyethylamine (B-HEAOL) and *N*-methyl-2-hydroxyethylamine (M-2HEAOL) on the surface of steel in 0.01 mol/L sodium chloride [Color figure can be viewed at wileyonlinelibrary.com]

TABLE 4 Variation in Reynolds number for various flow velocities in studied cases

μ (g·cm^{-1}·s^{-1})	ρ (g/cm^{-3})	U (cm/s)			
1.002×10^{-2}	0.998	13.08	26.17	52.33	104.67
		Re			
		1,303	2,606	5,212	10,424

PILs-containing solutions all over the experiment. Uninhibited steel presented some decrease in R_p during the test, starting with $2.8\,k\Omega \cdot cm^2$ and ending with $1.8\,k\Omega \cdot cm^2$, indicating that turbulent flow regime has a great influence on the corrosion behavior of uninhibited steel. This decrease in polarization resistance can be attributed to the increased transport of oxygen from the bulk to the metal surface by eddy diffusion. The rate of oxygen reduction reaction is generally limited by the speed at which oxygen can reach the surface of the metal. Previous studies[73–75] indicated that the greater

turbulence due to high velocities results in a more uniform O_2 concentration near the surface.[76]

In both PILs solutions, the steel presented higher values of R_p along the whole experiment. It seems that turbulence does not hamper the adsorption of the inhibitor that protects the sample from the first moments on, and so hindering the oxygen and chloride ions interaction with the steel surface. This behavior results in an inhibiting efficiency of over 90% for both PILs in turbulent flow conditions at all the studied rotations. Figure 4b–d show data for 500, 1,000, and 2,000 rpm, respectively. It can be seen that the corrosion behavior in each solution remained similar for all rotations. In this way, it is possible to assert that both inhibitors performance is not significantly affected by the flow regime, it means that the operational parameters and the consequent alteration of diffusion layer did not significantly affect the corrosive behavior of the studied systems, as the observed variations are within the margin of experimental error.[77]
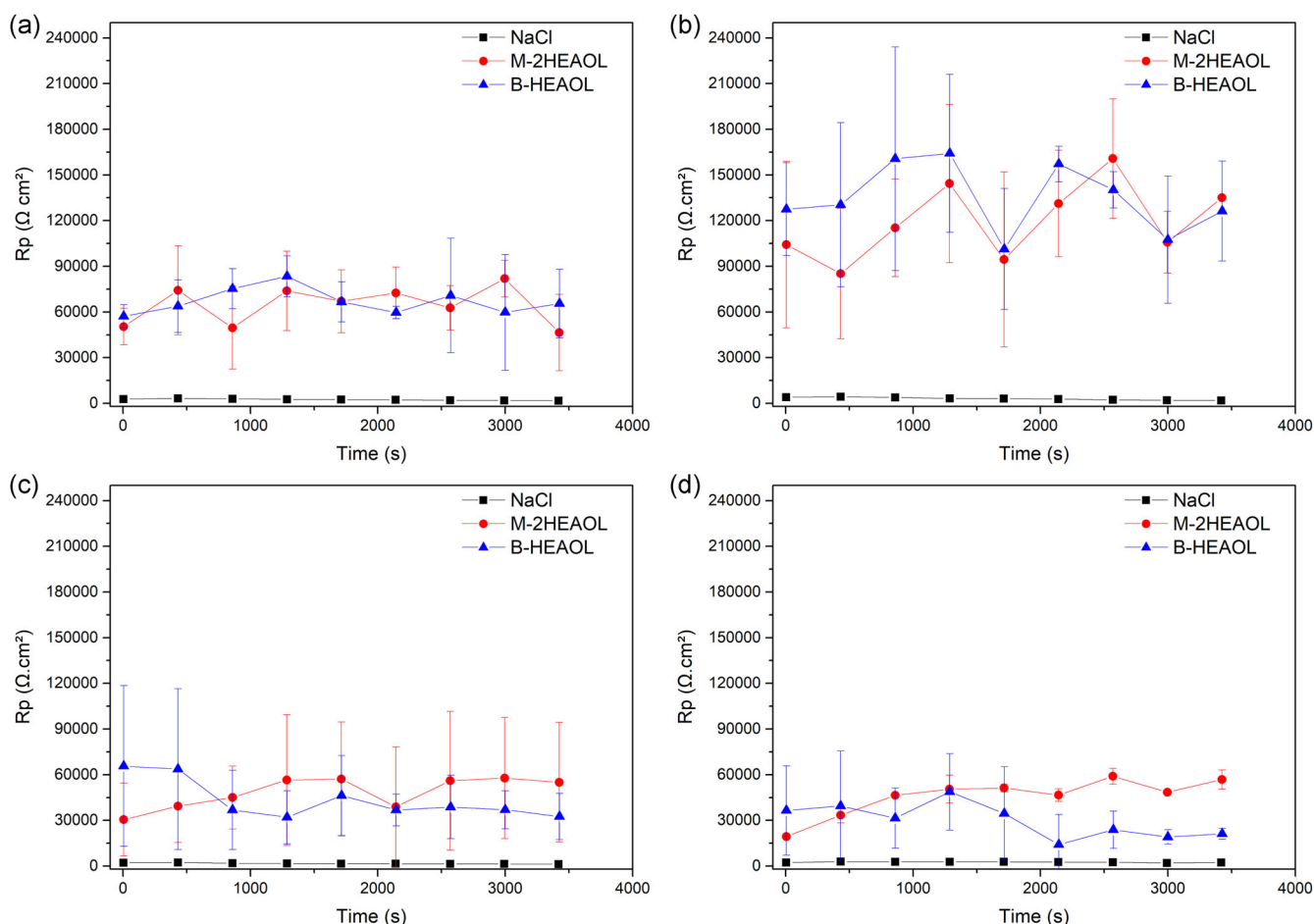
FIGURE 4 Evolution of R_p estimated by linear polarization resistance with increasing of time for (a) 250 rpm, (b) 500 rpm, (c) 1,000 rpm, (d) 2,000 rpm for three systems, 0.01 mol/L sodium chloride, 5 mmol/L M-2HEAOL + 0.01 mol/L sodium chloride, and 5 mmol/L B-HEAOL + 0.01 mol/L sodium chloride. B-HEAOL, bis-2-hidroxyethylamine; M-2HEAOL, *N*-methyl-2-hydroxyethylamine [Color figure can be viewed at wileyonlinelibrary.com]

3.6 | Cyclic voltammetry

Typical voltammograms for platinum in chloride solution are shown in Figure 5a. Three regions may be distinguished in the cyclic voltammetric curve of a Pt electrode in contact with an aqueous solution.[31,78,79] The region of lower potentials refers to hydrogen adsorption and desorption reactions. The "oxygen region" is found at positive potentials. During the positive sweep before O_2 evolution, a hydrated Pt oxide monolayer is formed (anodic current).[80] In the center of the voltammetric curve there is the double-layer a region where only low currents due to capacitive processes are found. This is the double-layer region where only capacitive processes take place. In the present work, it will be payed attention to the region pointed out as Peak 1 (Figure 5a), since all other peaks are suppressed with inhibitor addition and the goal of the employment of this technique was to evidence if there was adsorption or not of species on the working electrode. All voltammograms of this study are the first ones (without previous stabilization).

It can be seen that the hydrogen region is not clearly recognized at negative potentials and the oxygen reduction Peak 1 becomes smoother with the addition of the PIL's. To know if the reaction on Peak 1 was free-diffusion or adsorption-controlled, plots of i_p versus v and i_p versus $\sqrt[2]{v}$ were analyzed and are shown in Figure 6. In Figure 6a a straight line is formed with the plot of peak current versus square root of scan rate for uninhibited sodium chloride solution, with $R^2 = .9996$. So far, it can be concluded that the oxygen reduction for the system without inhibitor occurs in the free-diffusion regime. As for the case of B-HEAOL and M-2HEAOL in Figure 6b, a straight line is obtained from the plot of peak current versus scan rate, with R^2 of .9906 and .9783, respectively, which demonstrates that addition of both PILs changes the way how oxygen reacts, through an adsorption-controlled reaction.

So far, a direct link between the behavior on Pt electrode and steel electrode is not possible to make. However, it is possible to suggest that both ionic liquids affect the reactions of hydrogen and oxygen on Pt electrode.

3.7 | Surface analysis

Figure 7 presents the steel surface morphology before and after polarization tests in the presence and absence of inhibitor. Figure 7a,b shows steel surface of uninhibited steel (pH 6 and 9, respectively) after the corrosion test where an irregular morphology and corrosion marks all over the surface are observed, indicating severe damage on the metal. Figure 7c–h show the aspects for 5, 2.5, and 0.5 mmol/L M-2HEAOL and B-HEAOL, respectively. It is

observed the presence of a lower amount of corrosion products on the steel, (with the exception for the lowest concentration of B-HEAOL) where the structural damage is remarkably lower in comparison with the sample without both of PILs. Morphological analysis suggests the formation of a protective layer caused by the adsorption of PILs. In fact, corrosion is to be expected in all tested systems since samples were purposely polarized beyond breakdown potential, which was displaced in a positive direction, especially in 5 mmol/L.

Figure 8 shows three-dimensional images obtained from optical interferometry, where it is possible to note that the sample after the polarization curves in 0.01 mol/L sodium chloride (Figure 8b) had important alterations on topography due to corrosion. On the other hand, the samples in the different inhibited solutions (Figure 8c–h) had a single point of corrosion, most of the area remaining uncorroded. It is noteworthy that studied concentrations for both inhibitors produced almost imperceptible corrosion marks even in these accelerated corrosion tests.

Table 5 shows maximum depths of localized corrosion for each condition, where uninhibited steel presents 16 μm depth while in 5 mmol/L concentration for both PILs depth not more than 5 μm was found. The solution of 0.5 mmol/L concentration for M-2HEAOL showed the worse result, with 11 μm of depth. This result suggests that even in high anodic potentials, the corrosion of systems containing M-2HEAOL and B-HEAOL as CI is smoother than without PILs.

3.8 | FTIR-ATR spectroscopy

An infrared spectroscopy Fourier transform-ATR was used on samples immersed 20 days in 0.01 mol/L sodium chloride + 5 mmol/L M-2HEAOL, expecting this time allowed the inhibitor to act and form a thicker layer over the mild steel surface. Physical adsorption is usually reversible and the FTIR technique may be not able to detect it. However, when chemisorption occurs FTIR spectrometer is a powerful instrument that can be used to determine the type of bonding for organic molecules adsorbed on the surface of a solid.[81] An FTIR spectrometer was used (ex situ) to identify possible adsorption and to provide information on the new bond formation on the steel surface after immersion time. Figure 9 shows the FTIR spectrum of M-2HEAOL ionic liquid and the FTIR spectrum observed on the steel surface after it was exposed to 0.01 mol/L sodium chloride + 5 mmol/L M-2HEAOL for 20 days.

The spectrum of the inhibitor (M-2HEAOL) shows some characteristic vibrations in the 3,000–2,700 cm^{-1}
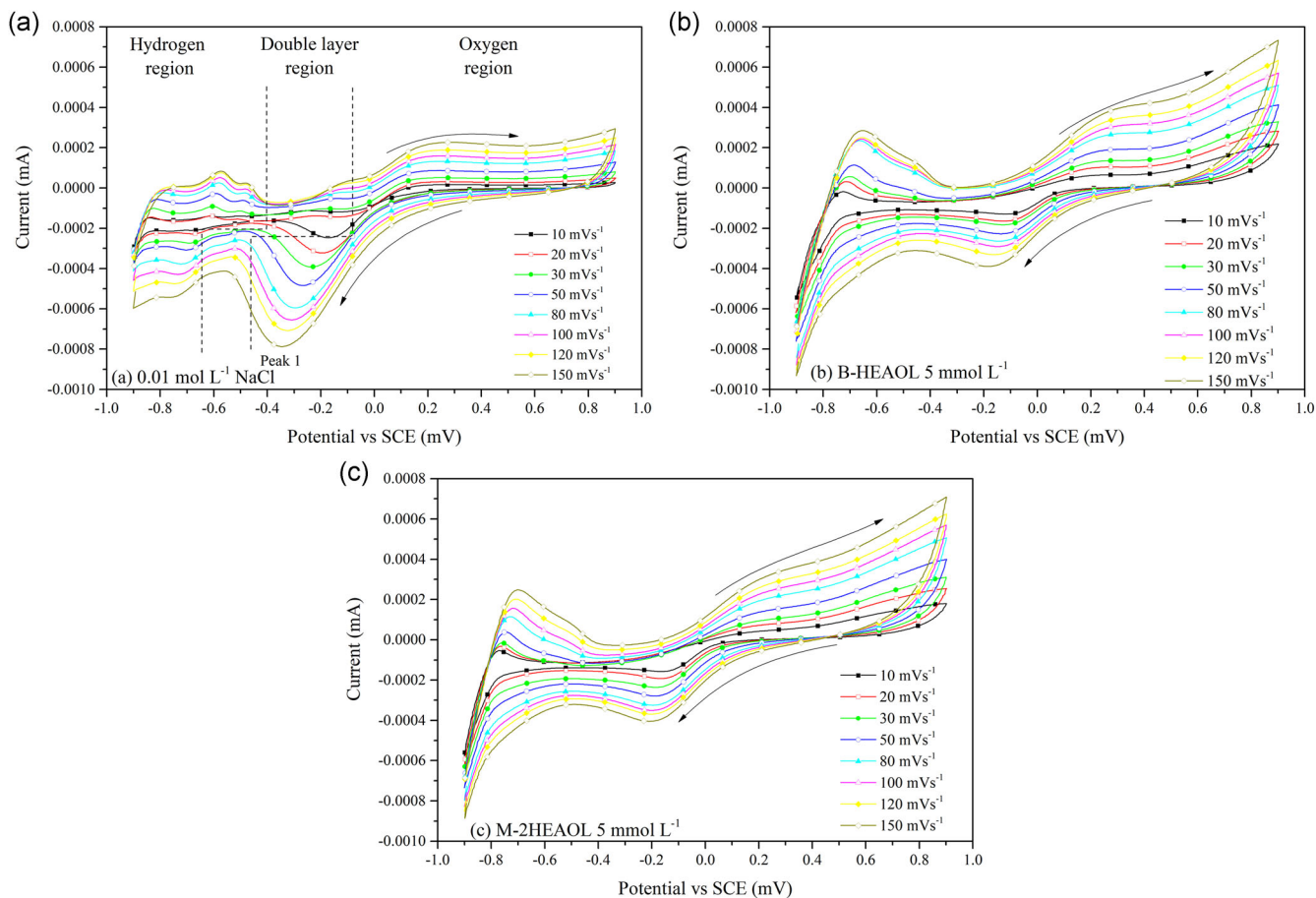
FIGURE 5 (a) Cyclic voltammetry of Pt in 0.01 mol/L sodium chloride solution on platinum substrate. (1) Peak evaluated, (b) cyclic voltammetry of Pt in 5 mmol/L M-2HEAOL + 0.01 mol/L sodium chloride, and (c) cyclic voltammetry in 5 mmol/L B-HEAOL + 0.01 mol/L sodium chloride. B-HEAOL, bis-2-hidroxyethylamine; M-2HEAOL, N-methyl-2-hydroxyethylamine [Color figure can be viewed at wileyonlinelibrary.com]
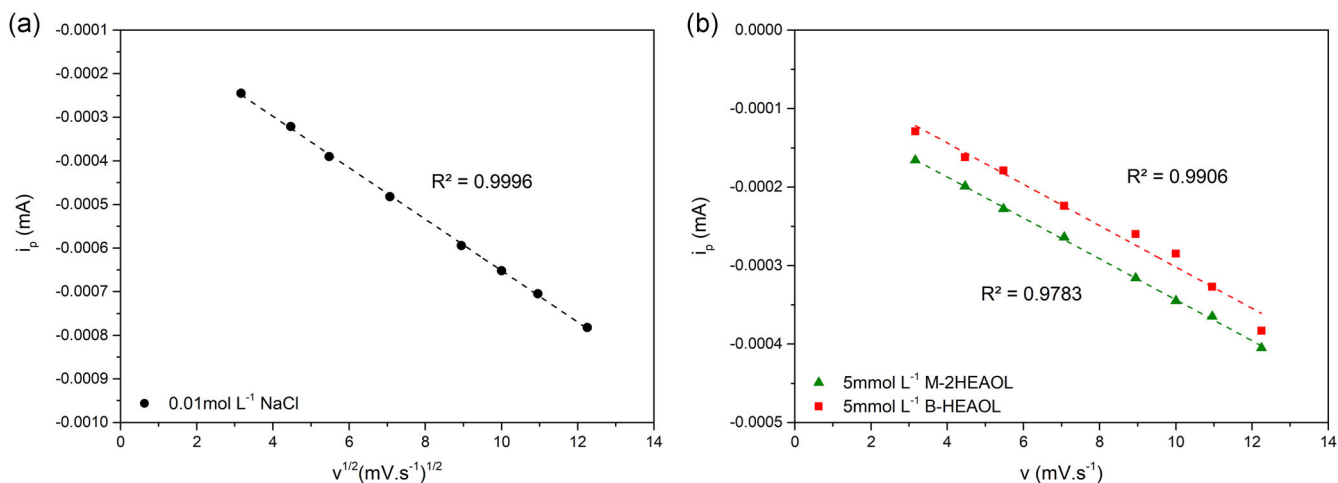
FIGURE 6 Peak current on Pt electrode versus square root of the scan rate for (a) 0.01 mol/L sodium chloride and (b) peak current versus scan rate for 0.01 mol/L sodium chloride + 5 mmol/L B-HEAOL and M-2HEAOL. B-HEAOL, bis-2-hidroxyethylamine; M-2HEAOL, N-methyl-2-hydroxyethylamine [Color figure can be viewed at wileyonlinelibrary.com]
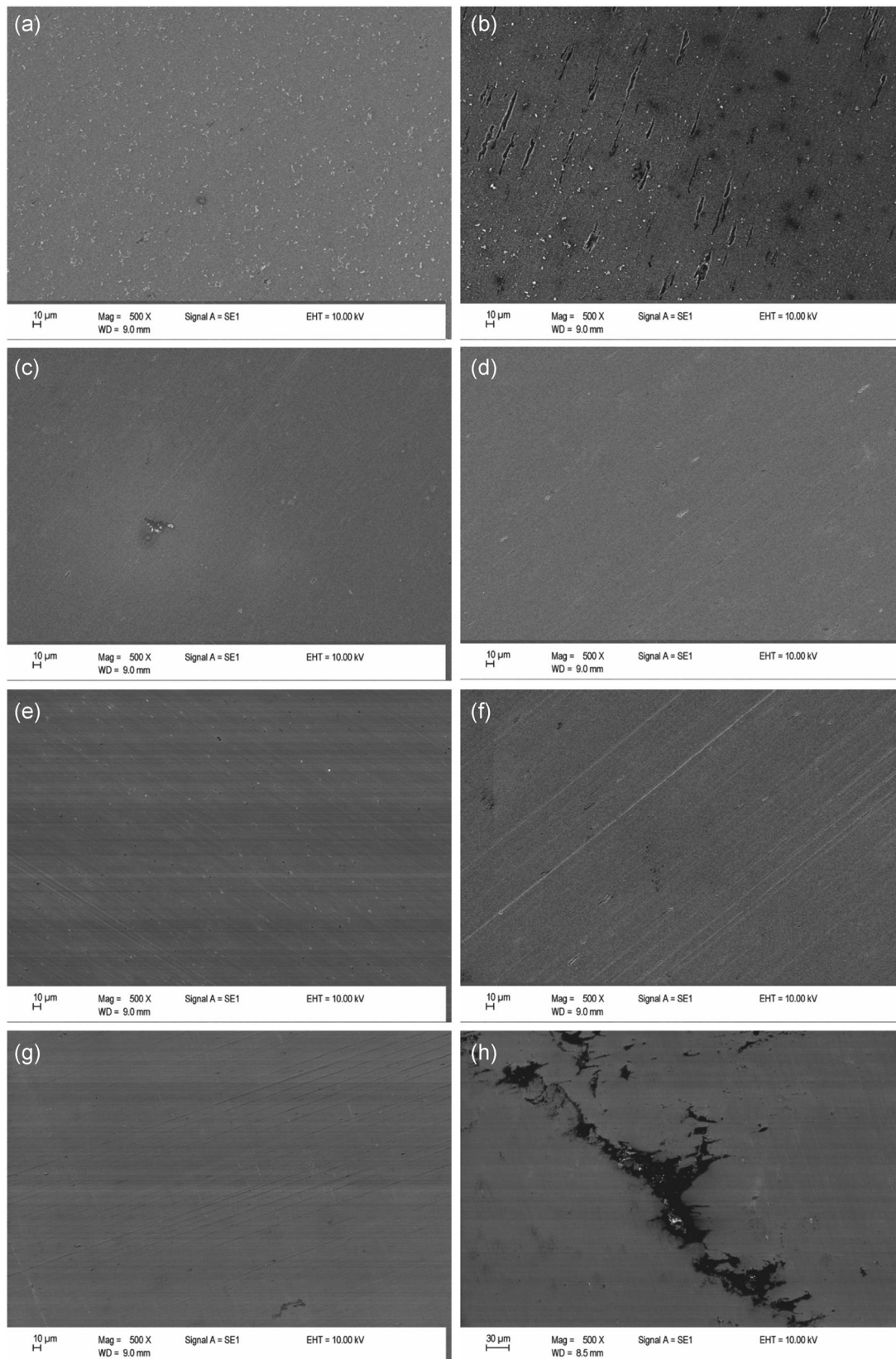
FIGURE 7 Scanning electron microscopy images after polarization tests of (a) 0.01 mol/L sodium chloride, pH 6, (b) 0.01 mol/L sodium chloride, pH 9, (c) 0.01 mol/L sodium chloride + 5 mmol/L M-2HEAOL, (d) 0.01 mol/L sodium chloride + 2.5 mmol/L M-2HEAOL, (e) 0.01 mol/L sodium chloride + 0.5 mmol L M-2HEAOL, (f) 0.01 mol/L sodium chloride + 5 mmol/L B-HEAOL, (g) 0.01 mol/L sodium chloride + 2.5 mmol/L B-HEAOL, and (h) 0.01 mol/L sodium chloride + 0.5 mmol/L B-HEAOL. B-HEAOL, bis-2-hidroxyethylamine; M-2HEAOL, *N*-methyl-2-hydroxyethylamine
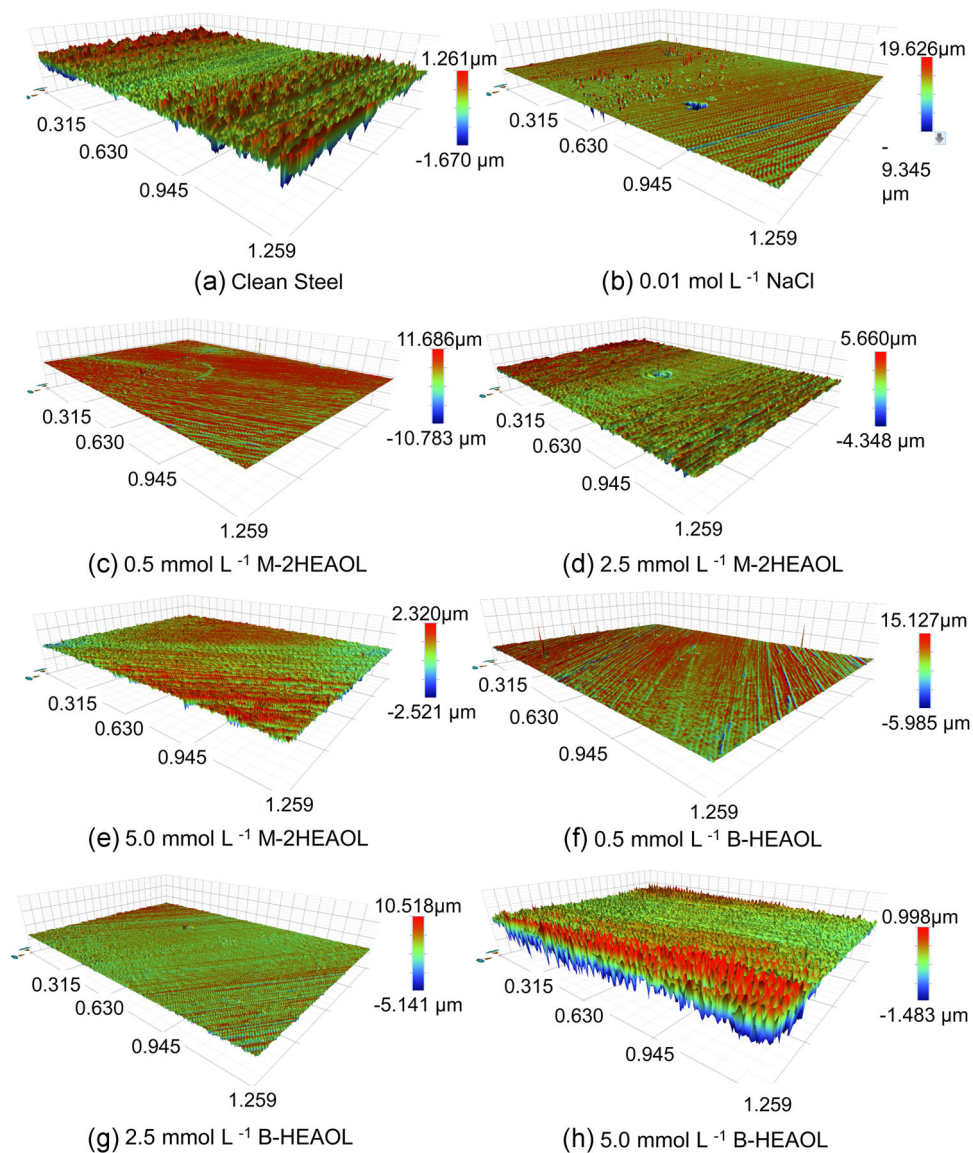
FIGURE 8 Topography obtained by optical interferometry for (a) clean steel and for steel after polarization curves in (b) 0.01 mol/L sodium chloride, (c) 0.01 mol/L sodium chloride + 0.5 mmol/L M-2HEAOL, (d) 0.01 mol/L sodium chloride + 2.5 mmol/L M-2HEAOL, (e) 0.01 mol/L sodium chloride + 5.0 mmol/L M-2HEAOL, (f) 0.01 mol/L sodium chloride + 0.5 mmol/L B-HEAOL, (g) 0.01 mol/L sodium chloride + 2.5 mmol/L B-HEAOL, and (h) 0.01 mol/L sodium chloride + 5.0 mmol/L B-HEAOL. B-HEAOL, bis-2-hidroxyethylamine; M-2HEAOL, *N*-methyl-2-hydroxyethylamine [Color figure can be viewed at wileyonlinelibrary.com]

TABLE 5 Maximum depth of localized corrosion for tested solutions

Test solutions	Maximum depth (μm)
0.01 mol/L NaCl	16
0.01 mol/L NaCl + 5.00 mmol/L M-2HEAOL	5
0.01 mol/L NaCl + 2.50 mmol/L M-2HEAOL	4
0.01 mol/L NaCl + 0.50 mmol/L M-2HEAOL	11
0.01 mol/L NaCl + 5.00 mmol/L B-HEAOL	3
0.01 mol/L NaCl + 2.50 mmol/L B-HEAOL	5
0.01 mol/L NaCl + 0.50 mmol/L B-HEAOL	4

Abbreviations: B-HEAOL, bis-2-hidroxyethylamine; M-2HEAOL, *N*-methyl-2-hydroxyethylamine.
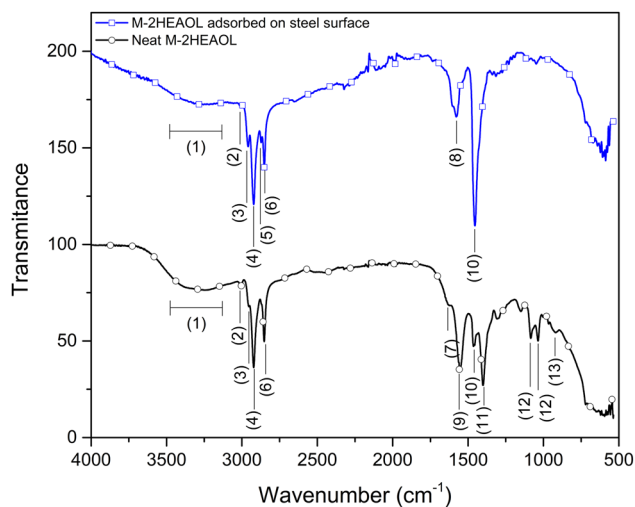
FIGURE 9 Fourier-transform infrared spectroscopy spectrum of M-2HEAOL ionic liquid and steel surface after 20 days exposition time in 0.01 mol/L sodium chloride + 5 mmol/L M-2HEAOL. B-HEAOL, bis-2-hidroxyethylamine; M-2HEAOL, *N*-methyl-2-hydroxyethylamine [Color figure can be viewed at wileyonlinelibrary.com]

TABLE 6 Characteristic infrared bands observed in studied systems

Peak number	Type of bonding	IR band	References
(1)	O–H	3,800–2,700	[82]
(2)	C=C–H	3,008	[83]
(3)	C–H from CH_3	2,960	[83]
(4)	C–H from CH_2	2,930–2,920	[83]
(5)	C–H from methyl	2,870	[83]
(6)	C–H from CH_2	2,850	[83]
(7)	NH_2 scissoring, N–H	1,615	[83]
(8)	C–O vibrations (e.g., in the –COOR groups)	1,578	[84,85]
(9)	N–H bending and C–N stretching	1,560–1,530	[83]
(10)	Alkoxide ion	1,455	[83,86,87]
(11)	=C–H	1,400	[83]
(12)	C–N	1,220–1,020	[83]
(13)	N–H	950–1,100	[83]

range. In the region between 2,960 and 2,850 cm^{-1}, vibrations associated with C–H single bonds were evidenced; moreover, at 2,850 cm^{-1} a vibration attributed to the C–H bond of the methyl radical was identified. Regarding the sp^2 bonds of carbon, they were identified at 3,008 cm^{-1} (C=C), as Table 6 summarized.

The band between 3,600 and 3,200 cm^{-1} is due to OH vibrations from the water molecule. At 1,560–1,530 cm^{-1} there are vibrations related to N–H bending (1,556 cm^{-1}), which are associated with the positively charged moiety of the liquid ionic (hydroxyethylammonium). In addition, the vibrations of the N–H bond also occurred at 1,084, 1,036, and 950 cm^{-1}.[82,83] In the range of 1,220–1,020 cm^{-1} were possibly associated with C–N binding that would be related to hydroxyethylammonium molecule. In relation to the structure of the oleate at 1,456 cm^{-1}, a peak associated with the vibration of the alkoxide ion is found; as identified in Table 6.

The FTIR spectrum obtained on the steel surface is quite similar to that of bulk M-2HEAOL spectrum (Figure 9), which indicates the presence of PIL on steel. The 3,000–2,700 cm^{-1} region did not present any difference in relation to the PIL spectrum. However, when the spectrum was analyzed at smaller wavenumbers, in the range of 1,600–1,400 cm^{-1}, other vibrations were observed, different from those observed only in PIL. One of the peaks associated with these vibrations occurred at 1,578 cm^{-1}, which was intense and may refer to ferric acetate, as previously reported by other authors.[84,85] It is also worth noting that at 1,456 cm^{-1} a very intense peak appears, which would be associated with the alkoxide ion that also

repeats in the ionic liquid spectrum and has already been reported by Oomens et al.[86,87]

The peaks associated with N–H binding occurring for the hydroxyethylammonium molecule were not identified on the ionic liquid spectrum when in contact with the steel surface; this would be a further indication that the probably coordinated bonding of the alkoxide ion with iron is predominant and occurs from the approximation of the oleate ion to the steel surface.

3.9 | Raman spectroscopic measurement

Raman spectra for the PIL M-2HEAOL can be found in Figure 10 (black line). The region between 2,800 and 3,000 cm^{-1} is related to the C–H vibration, which confirms the presence of the organic molecule on the metallic surface. The bands with center at 1,660 cm^{-1} correspond to the C=C present in the oleic acid [88] and the band at 1,443 cm^{-1} corresponds to deformations of the –CH_2– and –CH_3 functions coming from the cation moiety.[89] Bands at 1,304, 1,272, 1,088 cm^{-1} are related to the aliphatic chains present in both moieties of the PIL.[88,89]

Concerning the Raman spectrum obtained on the steel surface, the presence of the PIL is confirmed, since the same vibrations observed for the neat M-2HEAOL were
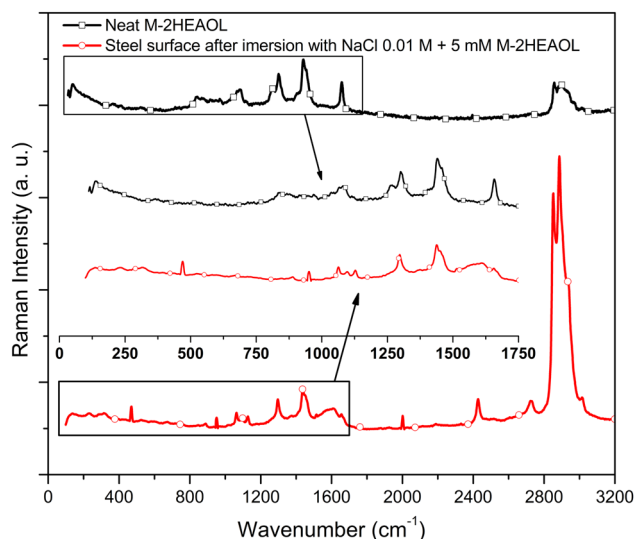
FIGURE 10 Raman spectra of M-2HEAOL ionic liquid and steel surface after 20 days exposition time in 0.01 mol/L sodium chloride + 5 mmol/L M-2HEAOL. B-HEAOL, bis-2-hidroxyethylamine; M-2HEAOL, N-methyl-2-hydroxyethylamine [Color figure can be viewed at wileyonlinelibrary.com]

observed for the steel sample after 20 days in contact with the inhibited sodium chloride solution. However, some peaks came to stronger evidence like that one at $2,400 \text{ cm}^{-1}$, peaks between 800 and $1,200 \text{ cm}^{-1}$ and a peak at 465 cm^{-1}, which can be related to hematite formation coming from the corrosion product, as well as to the formation of a coordination compound through the bond between the oxygen atom of the carboxylic function.[90] The peak at $1,660 \text{ cm}^{-1}$ appears convoluted in a broader one, which can be related to the coordination between the C=C bond and the steel surface as proposed elsewhere.[91]
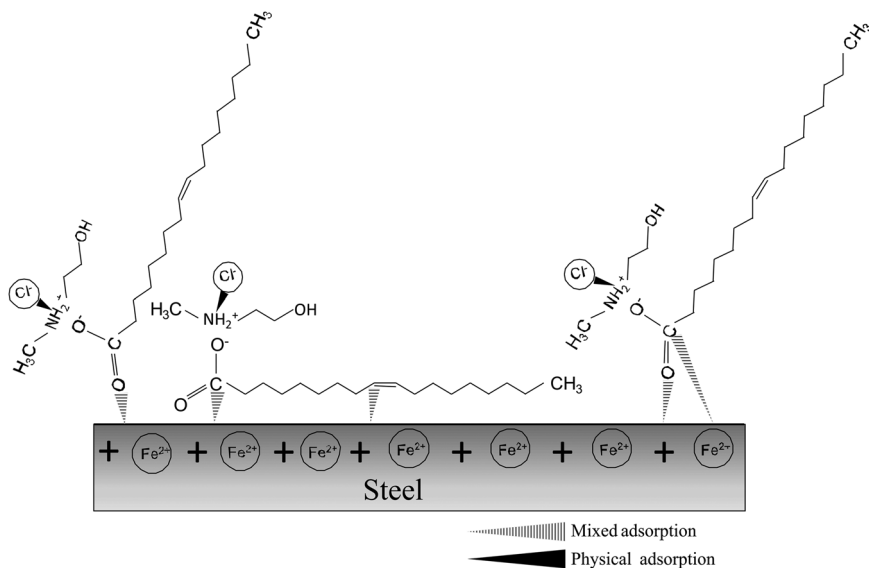
3.10 | Inhibition mechanism

A mechanism of ionic liquids corrosion inhibition is proposed as shown in Figure 11. Being the steel surface positively charged as shown by some authors[4,92] and associated with the greater electropositivity of Fe in relation to N, the approximation of the oleate ion to the metallic surface may occur through the oxygen negatively charged, establishing a mixed type adsorption (physisorption + chemisorption), as related to the results of Langmuir isotherms.

The peak at $1,578 \text{ cm}^{-1}$ on the M-2HEAOL Raman spectrum is related to C=O bonding; however, this peak suffered a reduction in its relative height, which means the impoverishment of this bond and the favoring of the formation of another one. As the positively charged ion of the ionic liquid (hydroxyethylammonium) undergoes destabilization and is forced to abandon the interaction with the oleate ion, the mixed adsorption process probably evolves into a coordinate type bond, favoring the formation of the Fe bond with oxygen, and consequently forming the iron oleate, as evidenced by the FTIR spectrum (Figure 9). Otherwise, the product formed can present the Fe-C bond due to the formation of a π bond between the d-π electrons of the iron atom and the antibonding orbital of the carboxylic function, which tends to lower the vibration of CO.[90] A metacarboxylic compound with a similar structure was formerly reported[86] and other authors report that this type of compound is usual to be formed on metal, and not on metal oxides.[93]

According to Szczepanski et al.,[94] the band due to the characteristic vibration of Fe:NH$_3$ is to be found at $1,130 \text{ cm}^{-1}$. Since this band was not observed on the FTIR spectra for the steel after contact with 0.01 mol/L

FIGURE 11 Schematic illustration of the corrosion mechanism of ionic liquid on carbon steel surface in 0.01 mol/L sodium chloride + 5 mmol/L M-2HEAOL. B-HEAOL, bis-2-hidroxyethylamine; M-2HEAOL, N-methyl-2-hydroxyethylamine

sodium chloride + 5 mmol/L M-2HEAOL, then the formation of Fe–N bond perhaps did not take place. It can be due to the steric hindrance caused by the presence of two chains of substituents in the amino function.[95,96]

On the other hand, C–N bands at 1,220–1,020 cm^{-1} present in the neat ionic liquid spectrum do not appear anymore in the spectra obtained for the specimen after immersion in the electrolyte containing M-2HEAOL. It can be due to the interaction of the chloride anion with the cation moiety of the PIL. It would explain that chloride does not reach the metal surface and consequently, the attack does not occur.

Regarding the wettability results, it was evidenced that after 30 min contact with the ionic liquid, the steel presented a more hydrophobic character (contact angle 90°) what could be associated with mixed adsorption of the oleate ion molecules on the steel surface. Such adsorption brings with it carbon chains that raise the apolar character of the surface, causing water molecules (polar) to fail to interact and form H bonds for greater hydrophilicity and higher surface energy to occur. After 20 days of exposure of the steel to the ionic liquid, there was an increase of the contact angle to 120° (Figure 1) and a visual aspect of grayish and opaque staining was verified due to a probable thickening of the layer of ionic liquid adsorbed on the surface. It is believed that the longer the exposure time of the steel surface to the ionic liquid, this thickening and increase of the mixed adsorption process may be associated with the continuous interaction of apolar oleate chains with new apolar ionic liquid molecules.[96]

Therefore, both PILs appear as promising substances to be employed as CIs, presenting efficiency superior to 93%, which puts them in a perspective of use in industrial sectors where high inhibition efficiency for long term is necessary. They worked out as mixed type adsorption inhibitors, with a predominantly anodic mechanism promoting a passive behavior at high concentration, with the presence of an adsorbed layer that blocked the attack of the electrolytic solution on the steel substrate.

4 | CONCLUSIONS

1. The addition of both PILs to the corrosive solution reduces the corrosion of AISI 1020 steel. Their inhibiting properties are due to the effect of physicochemical adsorption of the PILs molecules on the metallic substrate.
2. With the addition of PILs, the surface of the steel changes its characteristic of hydrophilic to hydrophobic, which enhances the substrate corrosion resistance.

3. Both studied PILs act as mixed type inhibitor with predominance on anodic reaction, and IE is favored by the increase in the concentration of the PILs. The IE values at the highest concentration (5 mmol/L) for M-2HEAOL and B-HEAOL reach up to 97%.
4. The difference on the surface morphology of uninhibited and inhibited mild steel surface is due to the formation of a protective layer as a consequence of PIL adsorption. Both PILs followed Langmuir isotherm, which best fitted the experimental data.
5. An inhibition mechanism based on all results has been proposed and PILs showing to act by adsorption through various functional groups of their molecule.
6. M-2HEAOL and B-HEAOL are able to increase polarization resistance of steel by up to 10 times in hydrodynamic conditions, independent of rotation speed.

ORCID

Tobias Eduardo Schmitzhaus 🄳 http://orcid.org/0000-0002-3667-8580
Maria R. Ortega Vega 🄳 http://orcid.org/0000-0002-6049-2831
Silvana Mattedi 🄳 http://orcid.org/0000-0003-4816-7494
Célia de Fraga Malfatti 🄳 http://orcid.org/0000-0002-0819-479X

REFERENCES

[1] A. L. Chong, J. I. Mardel, D. R. MacFarlane, M. Forsyth, A. E. Somers, *ACS Sustainable Chem. Eng.* **2016**, *4*, 1746.
[2] R. Touir, N. Dkhireche, M. Ebn Touhami, M. Lakhrissi, B. Lakhrissi, M. Sfaira, *Desalination* **2009**, *249*, 922.
[3] L.-B. Niu, K. Nakada, *Corros. Sci.* **2015**, *96*, 171.
[4] E. McCafferty, *Introduction to Corrosion Science*, Springer-Verlag, New York **2010**.
[5] C. Zuriaga-Monroy, R. Oviedo-Roa, L. E. Montiel-Sánchez, A. Vega-Paz, J. Marín-Cruz, J.-M. Martínez-Magadán, *Ind. Eng. Chem. Res.* **2016**, *55*, 3506.
[6] B. Bozzini, C. Mele, V. Romanello, *Mater. Corros.* **2007**, *58*, 362.

[7] Z. Tao, W. He, S. Wang, G. Zhou, *Ind. Eng. Chem. Res.* **2013**, *52*, 17891.

[8] C. Kamal, M. G. Sethuraman, *Mater. Corros.* **2014**, *65*, 846.

[9] I. B. Obot, N. K. Ankah, A. A. Sorour, Z. M. Gasem, K. Haruna, *Sustainable Mater. Technol.* **2017**, *14*, 1.

[10] M. A. Deyab, M. M. Osman, A. E. Elkholy, F. El-Taib Heakal, *RSC Adv.* **2017**, *7*, 45241.

[11] P. Arellanes-Lozada, O. Olivares-Xometl, N. V. Likhanova, I. V. Lijanova, J. R. Vargas-García, R. E. Hernández-Ramírez, *J. Mol. Liq.* **2018**, *265*, 151.

[12] S.-H. Yoo, Y.-W. Kim, K. Chung, N.-K. Kim, J.-S. Kim, *Ind. Eng. Chem. Res.* **2013**, *52*, 10880.

[13] M. Djellab, H. Bentrah, A. Chala, H. Taoui, *Mater. Corros.* **2019**, *70*, 149.

[14] G. Moretti, F. Guidi, F. Fabris, *Corros. Sci.* **2013**, *76*, 206.

[15] D. Liu, X. Qiu, M. Shao, J. Gao, J. Xu, Q. Liu, H. Zhou, Z. Wang, *Mater. Corros.* **2019**, *70*, 1907.

[16] I. Abdulazeez, O. C. Al-Hamouz, M. Khaled, A. A. Al-Saadi, *Mater. Corros.* **2020**, *71*, 292.

[17] M. R. O. Vega, K. Parise, L. B. Ramos, U. Boff, S. Mattedi, L. Schaeffer, C. F. Malfatti, *Mater. Res.* **2017**, *20*, 675.

[18] S. Mattedi, P. J. Carvalho, J. A. P. Coutinho, V. H. Alvarez, M. Iglesias, *J. Supercrit. Fluids* **2011**, *56*, 224.

[19] M. Iglesias, R. Gonzalez-Olmos, I. Cota, F. Medina, *Chem. Eng. J.* **2010**, *162*, 802.

[20] D. F. Kennedy, C. J. Drummond, *J. Phys. Chem. B* **2009**, *113*, 5690.

[21] M. E. Mashuga, L. O. Olasunkanmi, A. S. Adekunle, S. Yesudass, M. M. Kabanda, E. E. Ebenso, *Materials* **2015**, *8*, 3607.

[22] M. C. Bubalo, K. Radošević, I. R. Redovniković, J. Halambek, V. G. Srček, *Ecotoxicol. Environ. Saf.* **2014**, *99*, 1.

[23] M. R. Ortega Vega, J. Ercolani, S. Mattedi, C. Aguzzoli, C. A. Ferreira, A. S. Rocha, C. F. Malfatti, *Ind. Eng. Chem. Res.* **2018**, *57*, 12386.

[24] W. Zhang, H.-J. Li, A. Wang, C. Ma, Z. Wang, H. Zhang, Y.-C. Wu, *Mater. Corros.* **2020**, *71*, 498.

[25] M. A. Amin, K. F. Khaled, S. A. Fadl-Allah, *Corros. Sci.* **2010**, *52*, 140.

[26] M. A. Amin, M. M. Ibrahim, *Corros. Sci.* **2011**, *53*, 873.

[27] E. McCafferty, *J. Electrochem. Soc.* **1974**, *121*, 1007.

[28] Y. Zou, J. Wang, Y. Y. Zheng, *Corros. Sci.* **2011**, *53*, 208.

[29] ASTM G59-97, *Test Method for Conducting Potentiodynamic Polarization Resistance Measurements*, ASTM International, West Conshohocken **2014**.

[30] ASTM G185-06, *Practice for Evaluating and Qualifying Oil Field and Refinery Corrosion Inhibitors Using the Rotating Cylinder Electrode*, ASTM International, West Conshohocken **2016**.

[31] A. J. Bard, L. R. Faulkner, *Electrochemical Methods: Fundamentals and Applications*, Wiley, Austin **2000**.

[32] J.-M. Savéant, *Elements of Molecular and Biomolecular Electrochemistry: An Electrochemical Approach to Electron Transfer Chemistry*, John Wiley & Sons, New York **2006**.

[33] N. Elgrishi, K. J. Rountree, B. D. McCarthy, E. S. Rountree, T. T. Eisenhart, J. L. Dempsey, *J. Chem. Educ.* **2018**, *95*, 197.

[34] M. Pourbaix, *Corros. Sci.* **1972**, *12*, 161.

[35] V. Pandarinathan, K. Lepková, S. I. Bailey, T. Becker, R. Gubner, *Ind. Eng. Chem. Res.* **2014**, *53*, 5858.

[36] Y. Guo, B. Xu, Y. Liu, W. Yang, X. Yin, Y. Chen, J. Le, Z. Chen, *J. Ind. Eng. Chem.* **2017**, *56*, 234.

[37] I. B. Obot, A. Madhankumar, *Mater. Chem. Phys.* **2016**, *177*, 266.

[38] W. Villamizar, M. Casales, J. G. Gonzales-Rodriguez, L. Martinez, *Mater. Corros.* **2006**, *57*, 696.

[39] V. H. Álvarez, S. Mattedi, M. Martin-Pastor, M. Aznar, M. Iglesias, *Fluid Phase Equilib.* **2010**, *299*, 42.

[40] V. H. Álvarez, N. Dosil, R. Gonzalez-Cabaleiro, S. Mattedi, M. Martin-Pastor, M. Iglesias, J. M. Navaza, *J. Chem. Eng. Data* **2010**, *55*, 625.

[41] C. Li, *PhD thesis*, Ohio University, **2009**.

[42] H. E. Townsend, H. J. Cleary, L. Allegra, *Corrosion* **1981**, *37*, 384.

[43] C. Gabrielli, S. Joiret, M. Keddam, H. Perrot, N. Portail, P. Rousseau, V. Vivier, *J. Electrochem. Soc.* **2006**, *153*, B68.

[44] T. Liengen, R. Basseguy, D. Feron, I. Beech, *Understanding Biocorrosion: Fundamentals and Applications*, Elsevier, Amsterdam **2014**.

[45] M. Niinomi, *Metals for Biomedical Devices*, Elsevier, Amsterdam **2010**.

[46] F. Viejo, A. E. Coy, F. J. Garcia-Garcia, Z. Liu, P. Skeldon, G. E. Thompson, *Corros. Sci.* **2010**, *52*, 2179.

[47] A. K. Singh, S. Mohapatra, B. Pani, *J. Ind. Eng. Chem.* **2016**, *33*, 288.

[48] M. S. Al-Otaibi, A. M. Al-Mayouf, M. Khan, A. A. Mousa, S. A. Al-Mazroa, H. Z. Alkhathlan, *Arab. J. Chem* **2014**, *7*, 340.

[49] A. K. Singh, M. A. Quraishi, *Mater. Chem. Phys.* **2010**, *123*, 666.

[50] E. S. Ferreira, C. Giacomelli, F. C. Giacomelli, A. Spinelli, *Mater. Chem. Phys.* **2004**, *83*, 129.

[51] C. Wagner, W. Traud, Z. Für Elektrochem, *Angew. Phys. Chem.* **1938**, *44*, 391.

[52] E. McCafferty, *Corros. Sci.* **2005**, *47*, 3202.

[53] S. L. de Assis, S. Wolynec, I. Costa, *Electrochim. Acta* **2006**, *51*, 1815.

[54] C. J. Semino, J. R. Galvele, *Corros. Sci.* **1976**, *16*, 297.

[55] D. S. Azambuja, E. M. A. Martini, I. L. Müller, *J. Braz. Chem. Soc.* **2003**, *14*, 570.

[56] G. L. Makar, D. Tromans, *Corrosion* **1996**, *52*, 250.

[57] S. Javadian, B. Darbasizadeh, A. Yousefi, F. Ektefa, N. Dalir, J. Kakemam, *J. Taiwan Inst. Chem. Eng.* **2017**, *71*, 344.

[58] R. Solmaz, *Corros. Sci.* **2010**, *52*, 3321.

[59] F. S. Souza, A. Spinelli, *Corros. Sci.* **2009**, *51*, 642.

[60] S. P. Cardoso, F. A. dos Reis, F. C. Massapust, J. de Freitas Costa, L. S. Tebaldi, L. F. L. de Araújo, M. V. A. da Silva, T. S. de Oliveira, J. A. da Cunha Ponciano Gomes, E. Hollauer, *Quim. Nova* **2005**, *28*, 756.

[61] M. Bouklah, B. Hammouti, M. Lagrenée, F. Bentiss, *Corros. Sci.* **2006**, *48*, 2831.

[62] A. K. Singh, M. A. Quraishi, *J. Mater. Environ. Sci.* **2010**, *1*, 101.

[63] S. Kr. Saha, A. Dutta, P. Ghosh, D. Sukul, P. Banerjee, *Phys. Chem. Chem. Phys.* **2016**, *18*, 17898.

[64] R. Solmaz, *Corros. Sci.* **2014**, *79*, 169.

[65] R. Solmaz, *Corros. Sci.* **2014**, *81*, 75.

[66] A. Döner, R. Solmaz, M. Özcan, G. Kardaş, *Corros. Sci.* **2011**, *53*, 2902.

[67] A. O. Yüce, R. Solmaz, G. Kardaş, *Mater. Chem. Phys.* **2012**, *131*, 615.

[68] M. A. Deyab, M. T. Zaky, M. I. Nessim, *J. Mol. Liq.* **2017**, *229*, 396.

[69] M. A. Deyab, S. T. Keera, S. M. El Sabagh, *Corros. Sci.* **2011**, *53*, 2592.

[70] M. A. Amin, *J. Appl. Electrochem.* **2006**, *36*, 215.

[71] T. Douadi, H. Hamani, D. Daoud, M. Al-Noaimi, S. Chafaa, *J. Taiwan Inst. Chem. Eng.* **2017**, *71*, 388.

[72] A. Y. Musa, A. A. H. Kadhum, A. B. Mohamad, A. R. Daud, M. S. Takriff, S. K. Kamarudin, N. Muhamad, *Int. J. Electrochem. Sci.* **2009**, *4*, 707.

[73] Q. J. M. Slaimana, B. O. Hasan, *Can. J. Chem. Eng.* **2010**, *88*, 1114.

[74] Z. A. Foroulis, *Corrosion* **1979**, *35*, 340.

[75] P. V. Scheers, *J. South. Afr. Inst. Min. Metall.* **1992**, *92*, 275.

[76] B. O. Hasan, S. A. Sadek, *J. Ind. Eng. Chem.* **2014**, *20*, 297.

[77] S. Nesic, G. T. Solvi, S. Skjerve, *Br. Corros. J.* **1997**, *32*, 269.

[78] J. M. Doña Rodríguez, J. A. Herrera Melián, J. Pérez Peña, *J. Chem. Educ.* **2000**, *77*, 1195.

[79] H. Otmačić, J. Telegdi, K. Papp, E. Stupnišek-Lisac, *J. Appl. Electrochem.* **2004**, *34*, 545.

[80] M. Lukaszewski, M. Soszko, A. Czerwiński, *Int. J. Electrochem. Sci.* **2016**, *11*, 4442.

[81] H. Luo, Y. C. Guan, K. N. Han, *Corrosion* **1998**, *54*, 619.

[82] R. M. Silverstein, F. X. Webster, D. Kiemle, *Spectrometric Identification of Organic Compounds*, 7th., John Wiley & Sons, New York **2005**.

[83] B. H. Stuart, *Infrared Spectroscopy: Fundamentals and Applications*, John Wiley & Sons, New York **2004**.

[84] S. Karimi, J. Feizy, F. Mehrjo, M. Farrokhnia, *RSC Adv.* **2016**, *6*, 23085.

[85] A. Laurikėnas, J. Barkauskas, J. Reklaitis, G. Niaura, D. Baltrūnas, A. Kareiva, *Lith. J. Phys.* **2016**, *56*, 56. https://doi.org/10.3952/physics.v56i1.3274.

[86] H. G. M. Edwards, I. R. Lewis, *J. Mol. Struct.* **1993**, *296*, 15.

[87] J. Oomens, G. von Helden, G. Meijer, *J. Phys. Chem. A* **2004**, *108*, 8273.

[88] M. D. King, K. C. Thompson, A. D. Ward, *J. Am. Chem. Soc.* **2004**, *126*, 16710.

[89] Scfiner, Chemical Abstracts Service: Ethanol, 2-(Methylamino)-; Raman Spectra; Spectrum ID: RM56; RN : 141-43-5, National Institute of Advanced Industrial Science and Technology, 2019.

[90] K. Nakamoto, *Infrared and Raman Spectra of Inorganic and Coordination Compounds, Part B: Applications in Coordination, Organometallic, and Bioinorganic Chemistry*, John Wiley & Sons, New York **2009**.

[91] M. A. Hegazy, M. Abdallah, M. K. Awad, M. Rezk, *Corros. Sci.* **2014**, *81*, 54.

[92] H. H. Hassan, E. Abdelghani, M. A. Amin, *Electrochim. Acta* **2007**, *52*, 6359.

[93] G. Busca, V. Lorenzelli, *Mater. Chem.* **1982**, *7*, 89.

[94] J. Szczepanski, M. Szczesniak, M. Vala, *Chem. Phys. Lett.* **1989**, *162*, 123.

[95] J. de Damborenea, J. M. Bastidas, A. J. Vázquez, *Electrochim. Acta* **1997**, *42*, 455.

[96] T. Szauer, A. Brandt, *Electrochim. Acta* **1981**, *26*, 1253.